

# A Numerical Study of Tank Pressure Control in Reduced Gravity

Stephen Barsi\*

*Case Western Reserve University*

Mohammad Kassemi†

*National Center for Space Exploration Research*

Recent studies suggest that Zero Boil-Off (ZBO) technologies, aimed at controlling the pressure inside cryogenic storage tanks, will play a prominent role in meeting NASA's future exploration goals. Small-scale experiments combined with validated and verified computational models can be used to optimize and then to scale up any future ZBO design. Since shortcomings in previous experiments make validating comprehensive two-phase flow models difficult at best; the Zero Boil-Off Tank (ZBOT) experiment has been proposed to fly aboard the International Space Station. In this paper, a numerical model has been developed to examine several test points in the ZBOT test matrix. Specifically, a numerical model is developed to evaluate four pressure control strategies after the tank undergoes a period of self-pressurization. The four strategies include axial liquid jet mixing, mixing provided by a sub-cooled liquid jet, bulk liquid cooling provided by a cold-finger and cold-finger cooling with axial jet mixing. Results indicate, that over the time scales under consideration, sub-cooled liquid jet mixing is the most effective means to reduce tank pressure.

## Nomenclature

$c$	Specific heat	$\gamma$	Surface tension
$\vec{g}$	Gravity	$\mu$	Dynamic viscosity
$k$	Thermal conductivity	$\tau$	Viscous stress tensor
$L$	Latent heat	$\theta$	Transformed temperature
$M$	Molar mass	$\rho$	Density
$\dot{m}$	Mass flow rate		
$n$	Normal	<i>Subscripts</i>	
$p$	Pressure	$a$	Acrylic
$\dot{Q}_{IL}$	Interfacial heat power	$b$	Bubble
$q''$	Applied heat flux	$B$	Normal boiling point
$R$	Specific gas constant	$J$	Jet
$r$	Radius	$in$	Inlet
$T$	Temperature	$l$	Liquid
$t$	Time	$o$	Initial state
$\vec{V}$	Velocity	$out$	Outlet
$V$	Volume	$sat$	Saturation
		$ss$	Stainless steel
$\beta$	Expansion coefficient	$T$	Tank
$\delta$	Residual	$v$	Vapor

\*21000 Brookpark Rd., MS:105-1, Cleveland, OH 44135, AIAA Student Member

†AIAA Member

Copyright © 2006 by the American Institute of Aeronautics and Astronautics, Inc. The U.S. Government has a royalty-free license to exercise all rights under the copyright claimed herein for Governmental purposes. All other rights are reserved by the copyright owner.

## I. Introduction

Affordable and efficient cryogenic storage for use in propellant and life support systems is essential to meeting NASA's future exploration goals.<sup>1</sup> Significant cost and mass savings can be realized by improving cryogenic storage technology.<sup>2</sup> Cryogen mass losses can occur when heat leaks into the tank from the surrounding environment. When heat enters the tank, warmer fluid will be carried to the liquid vapor interface by natural convection currents. As the warmer fluid reaches the interface, evaporation will occur, resulting in vapor compression and a subsequent rise in tank pressure. Oftentimes, the tank pressure is relieved by venting. For on-surface applications, where the location of the vapor in the tank is well-defined, venting can easily be performed to reduce tank pressure. The situation is more complicated in reduced gravity environments where the vapor can conceivably be anywhere in the tank. In this case, liquid can be ingested into the vent line which can again result in a significant amount of cryogen mass loss. A strategy which has emerged as an alternative to direct venting is a zero boil-off system where a combination of forced liquid mixing and active cooling is used to control the tank pressure. A number of forced mixing concepts have been suggested: rotating impellers, radial or axial liquid jets,<sup>3</sup> and spray bars.<sup>4,5</sup> Cooling systems can be as varied. Suggested concepts include cryocoolers, heat pipes,<sup>6</sup> point-wise or distributed systems, and vapor cooled cryogen shields.<sup>7</sup>

Optimizing any future ZBO system requires careful consideration of the various mixing and cooling concepts and their effects on the underlying transport processes in the liquid and vapor. A flight-like demonstration with actual cryogenics is essential to understanding all of the complicated interactions involved in controlling tank pressure. Unfortunately, performing these tests can be costly and time consuming. An alternative approach to optimizing a ZBO system combines small scale model fluid experiments in both 1g and low g environments with detailed computational modelling. Data from the small scale fluid experiments can be used to validate, verify, and refine comprehensive two-phase numerical and analytical models. Once validated, the CFD models, along with the experimental data, will be used to scale up the ZBO design to a cryogenic flight system.

There have been several small scale experimental studies in both 1g and microgravity. These experiments could be classified into two categories: those where phase change was present and those where it was absent. In the latter category, investigations were typically concerned with slosh dynamics,<sup>8,9</sup> or mixing characteristics/flow profiles in the liquid.<sup>10-12</sup> The other category of experiments studied self-pressurization<sup>13</sup> and different pressure control strategies. In the 1990s, two shuttle experiments were conducted which looked at axial jet mixing as a means to control the tank pressure.<sup>14,15</sup> While the shuttle experiments met their stated objectives, there were some shortcomings to both experiments that prevented them from being used for model verification and validation. First, contaminant species leaked into the test cell either before or during the experiment. It is unclear whether any of the data sets corresponded to pure liquid/vapor cases. While the authors claim that the contaminant species (which were estimated at 2% mass fraction) did not have any effect on the data, recent work by Panzarella and Kassemi<sup>16</sup> suggest that even trace amounts of contaminants can have an adverse effect on the condensation rate. Second, the two heaters in the shuttle experiments were submerged in the tank away from the wall. Heat sources submerged in the liquid produce bulk heating that has quite different flow and heat transfer dynamics than the actual boundary layer flows that result when heat leaks in through the tank wall. Third, the heating and mixing phases of the experiment were too short to yield any meaningful comparisons to thermodynamic predictions of the self-pressurization rate. Comparison to the thermodynamic pressure rise rate is only meaningful when a stationary thermal state prevails in the liquid. Unfortunately in both shuttle experiments, heating and mixing were only performed over a time scale of minutes. The results presented herein and elsewhere<sup>17-19</sup> indicate that the time scales associated with reduced gravity self-pressurization and/or mixing can be on the order of hours or even days. Clearly, after running the experiment for only a few minutes, temperature and flow field transients were still developing and comparisons with the thermodynamic solution would be meaningless.

Also, it is unclear if any rigorous thermal controls were imposed on the experiment. The thermal conductivity of the tank wall was greater than the conductivity of both the liquid and vapor. If any thermal energy reached the wall, some would have been absorbed in the wall and some might have been lost to the surrounding environment. Yet no attempt to quantify this potential thermal loss was made. Moreover, no temperature controls were placed on the mixing jet. The simulations presented here indicate that sub-cooled liquid jet mixing results in significantly different pressure decay behavior than if the jet were not sub-cooled. This uncertainty in jet inlet temperature was not quantified in either of the shuttle experiments. Finally, it is unclear whether subsequent experimental runs began from the same thermodynamic state since subsequent

runs began only after waiting several minutes between the mixing and heating phases of the experiment. This is not satisfactory since the above condition implies that subsequent runs can begin from a different state along the saturation curve. This ambiguity in the initial state is important because for a given heat load, one would detect a steeper pressure rise if the experiment were started on a steeper section of the saturation curve. These experimental shortcomings make validating and verifying a numerical model difficult, if not, impossible; so to resolve these inadequacies, the Zero Boil-Off Tank (ZBOT) experiment has been proposed to fly aboard the International Space Station. Data from the ZBOT experiment will be used to validate our comprehensive two-phase flow numerical and analytical models.

Following our hand-in-hand numerical/experimental approach to studying cryogenic fluid management, a computational model has been developed to investigate different cooling and mixing scenarios that will be performed during the ZBOT experiment. Historically, cryogenic tank modelling has proceeded along three fronts. Initially, thermodynamic models were developed to understand tank self-pressurization.<sup>13,20,21</sup> While thermodynamic models do an adequate job of predicting the self-pressurization rate,<sup>22</sup> many finer details of the pressurization history are lost since thermodynamic models assume spatially uniform temperature and pressure fields and cannot resolve any gradients in the domain or capture any initial transients in the solution.

To resolve some of these shortcomings, the next tier of sophistication involved integrating the conservation equations over a fully developed natural convection boundary layer.<sup>23-26</sup> While the results based on this boundary layer formulation have been met with some success, the limitations of this model involve relatively simple tank and interface geometries and of course well-defined boundary layer flows along the tank wall.

For more complicated geometries and flow patterns, detailed computational models have been developed to study cryogenic fluid management. Previous numerical simulations have typically been limited to studying isothermal phase distribution<sup>27-30</sup> or temperature and flow behavior in the liquid while neglecting any phase change at the liquid vapor interface.<sup>31-35</sup> Recently, attempts have been made to couple phase change at the interface to the temperature and flow fields in the liquid.<sup>22,36,37</sup>

In the present paper, similar to the Panzarella and Kassemi formulation,<sup>22</sup> a lumped mass and lumped energy formulation of the vapor is coupled to the time dependent conservation equations in the liquid. The system of equations is solved using a finite volume formulation developed in-house. After self-pressurizing the tank for 12 hours with an applied heat load of 0.5 W, the CFD model is used to investigate four pressure control strategies. In the first case study, an axial jet mixer is used to disrupt the thermal stratification near the interface. In this case, the jet provides no cooling and is only used to mix the bulk liquid. For the second case study, again an axial jet is used to mix the bulk liquid but now, the liquid that enters the tank is subcooled. While this will be shown to be an effective means to reduce tank pressure, from a reliability and power consumption standpoint, it is not practical in actual flight systems to continuously run the jet mixer for long periods of time. Consequently, in the third case study, cooling is provided by a cold-finger submerged in the liquid and the jet mixer is turned off. Any mixing in this case is limited to natural convection. Finally, in the fourth case study, a combination of cold-finger cooling and jet mixing is employed. In this case, the jet itself provides no cooling and is only used to mix the liquid. The effectiveness of these four strategies in controlling tank pressure will be discussed and analyzed.

## II. Mathematical Model

This paper analyzes several test points in the ZBOT test matrix. The experimental apparatus is shown in Figs. 1 and 2. The test cell is 4" x 8" (diameter x length). The cylindrical body and top hemisphere is made of acrylic. The bottom hemisphere is made of stainless steel. Both sections of the tank wall are 1/8" thick. A nozzle (3/8" diameter) projects 2" into the test cell. A cold-finger ring is located 1" downstream of the jet nozzle. The ring diameter is 1.5" and is centrally located about the axis of symmetry. The entire outer wall is adiabatic except for two strip heaters affixed to the outer wall of the test cell. The heaters are 1/2" wide and are located on the cylindrical section of the tank wall where the top and bottom hemispheres mate with the central cylinder. For all the case studies presented here, 0.25 W is distributed uniformly over each heater. The volumetric liquid fill fraction is 95%. The vapor is contained in a spherical bubble lying along the center line 3/16" away from the apex of the top hemispherical dome. For all the cases studied, both the shape and location of the vapor region are fixed. The validity of this simplifying assumption will be discussed later. The model fluid used in the ZBOT experiment is HFE-7000, a low boiling point transparent refrigerant with a relatively steep saturation curve. Relevant thermophysical properties are listed in Table

1.

The liquid is treated as an incompressible, Newtonian, Boussinesq fluid whose flow field can be described by the continuity and Navier-Stokes equations:

$$\nabla \cdot \vec{V} = 0 \quad (1)$$

$$\rho \left( \frac{\partial \vec{V}}{\partial t} + \vec{V} \cdot \nabla \vec{V} \right) = -\nabla \tilde{p} + \nabla \cdot \tau - \rho \vec{g} \beta \theta \quad (2)$$

In the momentum equations,  $\theta$  is a transformed temperature field and is defined in terms of a deviation from the saturation temperature:

$$\theta(\vec{x}, t) = T(\vec{x}, t) - T_{sat}(t) \quad (3)$$

The pressure appearing in the momentum equation is a combination of the thermodynamic pressure and any hydrostatic contribution:

$$\tilde{p} = p - \rho \vec{g} \cdot \vec{r} \left( 1 - \beta \left[ T_{sat}(t) - T_{sat}(0) \right] \right) \quad (4)$$

Conservation of energy can be described by:

$$\rho c \left( \frac{\partial \theta}{\partial t} + \vec{V} \cdot \nabla \theta \right) = \nabla \cdot (k \nabla \theta) - \rho c \frac{dT_{sat}}{dt} + \tau : \nabla \vec{V} \quad (5)$$

The second term on the right side appears because of the variable transformation given in equation (3). The last term on the right side is a heat source due to viscous dissipation which may or may not be important at very fast jet speeds.

The vapor is treated as a lumped inviscid, compressible, ideal gas whose pressure, density and temperature are spatially uniform. An energy balance in the vapor (neglecting kinetic energy, gravitational potential energy and viscous dissipation) leads to:

$$\frac{dp_v}{dt} \left\{ \rho_v c_v V_v \frac{\partial T}{\partial p} - \frac{\partial(\rho_v V_v)}{\partial p} \left[ p_v \left( \frac{1}{\rho_v} - \frac{1}{\rho_l} \right) - L \right] \right\} = \dot{Q}_{IL} \quad (6)$$

where  $\rho_v$  is the vapor density:

$$\rho_v(p_v) = \frac{p_v}{RT(p_v)} \quad (7)$$

$T$  is the vapor temperature and is related to the vapor pressure through the Clausius-Clapeyron equation:

$$T(p_v) = \left[ \frac{1}{T_B} - \frac{R}{L} \ln \left( \frac{p_v}{p_B} \right) \right]^{-1} \quad (8)$$

and the vapor volume can be found by integrating the global mass conservation equation:

$$V(p_v) = V_o \frac{\rho_l - \rho_{v,o}}{\rho_l - \rho_v} \quad (9)$$

A more complete derivation is given in Panzarella and Kassemi.<sup>22</sup>

The lumped vapor model is coupled to the solution in the liquid through the interfacial heat power,  $\dot{Q}_{IL}$ . First, the solution in the liquid is obtained. The temperature field is used to compute the interfacial heat power on the liquid side of the interface. This is then used to evolve the vapor pressure in time. The new vapor pressure imposes a new saturation temperature along the interface. The new interfacial temperature changes the heat flux at the interface which when integrated over the interfacial area changes the heat power entering (or leaving) the vapor. Iteration proceeds until convergence is attained.

The tank is heated by prescribing a steady heat flux uniformly over the section of outer tank wall where the heating strips are located. The heat flux is defined so that a net heat power of 0.5 W is prescribed. Along the rest of the outer tank wall, the nozzle body, and the outlet body adiabatic conditions are applied. At all fluid-solid interfaces, no-slip and impermeability constraints are applied. Along the tank outlet and jet inlet, adiabatic conditions are prescribed when the jet is inactive. When the jet is active, a parabolic velocity

profile is prescribed at the inlet and two temperature conditions can either be applied. For sub-cooled jet mixing, the temperature of the incoming liquid stream is known:

$$\theta_J = T_J - T_{sat}(t) \quad (10)$$

In the mixing only case when the jet is only used to mix the bulk liquid, the temperature at the jet inlet is found by performing an energy balance between the tank outlet and jet inlet:

$$\sum_{out} \dot{m}cT = \sum_{in} \left( \dot{m}cT - kS \frac{\partial T}{\partial n} \right) \quad (11)$$

where the summation on the left side of the equation is applied over all outlet cell faces, and the summation on the right is applied over all inlet cell faces. Using the above equation to solve for the inlet temperature can be considerably simplified by assuming the temperature is uniform over the inlet area. Once the inlet temperature is known then, once again, equation (10) is used to prescribe the condition on  $\theta$ .

As can be deduced from equation (11), along the outlet boundary diffusive contributions in the energy equation are set to zero:  $\nabla T \cdot \hat{n} = \nabla \theta \cdot \hat{n} = 0$ . The velocity at the outlet is defined so that the liquid is removed from the tank at the same mass flow rate as the incoming liquid jet.

Generally, the liquid-vapor interface is a deformable surface separating two distinct phases. Moreover, the location of the interface is typically not known *a priori*. To simplify the current analysis, we fix both the shape and the location of the interface. If the vapor region were initially situated in the center of the tank then, similar to the results of Panzarella *et al.*,<sup>18</sup> the vapor would migrate to one end of the tank due to buoyancy. In a  $9.81 \cdot 10^{-6} \text{ m/s}^2$  acceleration field this migration time can be estimated from  $\sqrt{\frac{2d}{g}}$  where  $d$  is the distance between the ullage and the tank wall. For a vapor bubble initially located at the center of the tank,  $d = 3.5''$  and the migration time is thus 135 seconds. In this time, heat has barely conducted through the tank wall and begun to penetrate into the liquid. Since thermal energy has not yet reached the interface, the pressure would not yet have begun to rise. Furthermore, similar to many cryogenics, HFE-7000 is a wetting fluid. When the rising vapor bubble hits the tank wall it would likely retract owing to a combination of surface tension forces and wettability. Because it is unlikely that the vapor pressure would have significantly changed during the migration time and because a liquid layer is likely to form between the ullage and the tank wall, the location of the ullage is fixed near the top of the tank opposite the direction of the residual gravity vector.

Once the initial position of the ullage is set, the shape of the vapor volume can change in several ways. First, the shape of the ullage would change if significant mass transfer were occurring at the interface. If evaporation were occurring, for example, and enough mass were transferred from the liquid into the vapor, then the interface would noticeably recede into the liquid. For the experimental conditions considered here, the net mass transferred at the interface is very small. After self-pressurizing the tank for 12 hours with a heat load of 0.5 W, the net mass transferred from the liquid into the vapor is 0.12 g. This corresponds to a negligible change in vapor volume and thus a negligible change in the radius of the ullage bubble (0.04%).

The shape of the interface can also change when the liquid jet impinges the surface. One can imagine several scenarios: the jet can flow smoothly around the interface having no effect on the shape; the jet can cause a small indentation in the interface at the point of impingement; or the jet can geysir into the vapor and re-enter the liquid at the opposite end of the ullage. The likelihood of these scenarios occurring can typically be quantified in terms of the Weber number  $\left( \frac{\rho_l u_J^2 r_J^2}{2\gamma r_T} \right)$ : the ratio of the jet's inertia to the restoring effects of surface tension. For the experimental conditions presently considered ( $u_J = 0.1 \text{ cm/s}$ )  $We = 2.5 \cdot 10^{-5}$ , thus surface tension forces dominate and the jet is likely to have little effect on the shape of the interface. So to simplify the analysis, the shape of the initially spherical ullage is fixed throughout the simulation.

To summarize, both the shape and location of the interface are fixed throughout the analysis. In the momentum equations two boundary conditions are applied at the interface. First, fluid is allowed to slip over the surface by applying a shear free condition at the interface. Second,  $\vec{V} \cdot \hat{n} = 0$  is enforced at the interface. This condition is a consequence of a static interface when the net mass transferred across the surface is small. Finally for the energy equation, the saturation temperature is applied uniformly over the interface.

### III. Numerical Methodology

To solve this problem numerically, a finite volume model for the problem is developed in house. In this primitive variable formulation, all variables are defined at the cell centers. The standard Rhie and Chow correction<sup>38</sup> is used to define mass fluxes at the cell faces. Moreover, corrections due to grid non-orthogonality are also employed when computing cell-face fluxes. The SIMPLE<sup>39</sup> pressure correction method is used to update the pressure field. The scheme is nominally second order accurate employing a combination of up-winding and central differencing in a deferred correction approach to spatial derivatives with second order multi-level time integration. For a general overview of the numerical methodology employed for this problem see Ferziger and Peric.<sup>40</sup>

The coupled system of equations is solved sequentially using Stone's semi-implicit procedure.<sup>41</sup> Convergence of the inner iterations is achieved when

$$\left\| \frac{\delta_\phi}{\delta_{\phi,o}} \right\| < 0.02 \quad (12)$$

where  $\delta$  is the L1 norm of the residual vector and  $\phi$  can be  $u$ ,  $v$ ,  $p$ , or  $\theta$  depending on which sub-system is currently being solved. Before proceeding to the next time step, the following outer iteration convergence criteria is enforced:

$$\left\| \max \left( \delta_u, \delta_v, \delta_p, \delta_\theta \right) \right\| < 10^{-8} \quad (13)$$

The inner iteration convergence criteria is much weaker because the conservation equations are coupled together through the buoyancy term in equation (2) and the computed solution may change from one outer iteration to the next. All of the computations are started from a motionless state with a uniform temperature of  $T_{sat}$  ( $\theta = 0$ ).

The solutions presented in this paper are generated using 8168 control volumes (CVs) with a dense clustering of CVs near the jet inlet, liquid-wall and liquid-vapor interfaces so that any thermal or momentum boundary layers that may develop at these boundaries can be resolved. Grid resolution was checked by comparing solutions generated on four grids with 1974, 4799, 8168, and 16015 CVs respectively. Representative examples of the grid resolution are presented in Fig. 3 for the final vapor pressure after self-pressurizing for 12 hours. Comparisons indicate excellent grid resolution.

### IV. Results

In order to evaluate the four pressure control strategies analyzed in this paper, first a tank partially full of HFE-7000 is allowed to self-pressurize under a constant heat load of 0.5 W uniformly distributed over two strip heaters affixed to the outer wall of the tank. The volumetric liquid fill fraction is 95% and the spherical ullage bubble is fixed at the end of the tank opposite the direction of the residual gravity vector. Time sequences of the temperature and velocity fields in the liquid during self-pressurization are shown in Fig. 4. In order to conserve space and because the solution is axisymmetric, the two fields are combined into a single plot with the isotherms on the left and the velocity vectors on the right.

As shown in Fig. 4, heat enters the liquid through the tank wall near where heat is being supplied by the strip heaters. Natural convection currents generated by density differences in the liquid carry this heat up along the tank wall towards the interface. Convective vortices develop at the side wall near the location of heat input. After carrying warmer fluid up towards the ullage, fluid is drawn down along the tank centerline to supply the upwardly traveling boundary layer flow at the wall. The maximum convective speed is on the order of microns/sec. Since the Rayleigh number describing this flow  $\left( \frac{\rho_l^2 c_l g \beta q'' r_T^4}{k_l^2 \mu_l} = 8397 \right)$  is small, as expected, the natural convection in the tank is laminar.

As shown in Fig. 4a, it takes a little less than 1 hour before heat energy entering the liquid is carried to the interface. After self-pressurizing for 6 hours, thermal stratification begins to develop in the liquid. At 12 hours, there has been little change in the velocity field and a thermally stationary state is beginning to develop. Once a stationary state is achieved, the temperature of the liquid will continue to increase with heating, but temperature gradients in the liquid will become temporally constant resulting in a constant pressurization rate. Once heating begins, a lag in the pressurization response is initially observed as shown in Fig. 5. This lag is due to the finite amount of time it takes heat to be carried to the interface. The

lag is more pronounced in microgravity than in terrestrial environments because of the slower convective speeds. Once heat reaches the ullage, evaporation occurs and the vapor pressure begins to rise. Initially, the pressurization rate will be non-uniform because of transients in the liquid caused by developing thermal fields. As the thermal field becomes more developed, the pressurization rate will tend towards a constant as dictated by thermodynamics.

In 1g, strong natural convection mixes the bulk liquid which effectively wipes away any local hot spots in the domain. In microgravity, because of the slower convective speeds combined with the low thermal conductivity of the test liquid, larger superheats can be supported. For the present experimental configuration, the maximum superheat, after self-pressurizing for 12 hours, is 4.3176 K and is located adjacent to the tank wall near the upper strip heater. Liquid adjacent to the tank wall near the bottom heater is slightly cooler because the warmer fluid is being carried upwards by natural convection.

The four pressure control strategies analyzed here all begin after self-pressurizing the tank for 12 hours. The heaters remain active during the 2 hours the mixer and/or cooler is on. In the first case study, we attempt to reduce the tank pressure by disrupting the thermal stratification in the liquid with an axial jet mixer. In this case, the axial liquid jet only mixes the bulk liquid; no energy is removed between the tank outlet and jet inlet. For this case, and all subsequent jet cases, the average jet speed at the inlet is 0.1 cm/s. This corresponds to a jet Reynolds number,  $\frac{\rho U_{jet} r_j}{\mu}$ , of 14.8.

A time sequence of the temperature and velocity fields for the mixing-only case is shown in Figure 6. In order to reach the interface, the upwardly traveling mixing jet must overcome the buoyancy-induced flow that is pulling fluid down along the centerline of the tank. However, since the average jet speed in the present case is several orders of magnitude greater than the largest natural convection speed, the liquid jet easily overcomes the opposing buoyant flow. As shown in Fig. 6a, 90 seconds after the jet is turned on, the liquid jet still has not reached the interface but the plotted temperature field indicates that the jet is carrying cooler fluid up towards the ullage. The cooler jet fluid is not a result of any active cooling. Rather, the jet is pulling cooler fluid that has settled to the bottom of the tank up towards the ullage. When the colder fluid reaches the interface, condensation will begin and, as shown in Fig. 10, the vapor pressure will decrease. After approximately 10 minutes, the liquid jet has already reached the interface. The isotherms shown in Fig. 6b, suggest that the recirculating jet flow is pulling warmer fluid from the bottom heater radially inward. When this warmer fluid gets entrained with the jet, which carries it to the interface, evaporation will occur and the vapor pressure will begin to rise again. Two hours after the jet is turned on, as indicated by the isotherms in Fig. 6d, the axial jet mixer does an adequate job at destratifying the liquid. Unfortunately, since no energy has been removed from the tank, the vapor pressure continues to increase. The short-term drop in pressure shown in Fig. 10, is a result of bringing the cooler fluid that has settled to the bottom of the tank up towards the interface. To sustain this pressure reduction, energy must be removed from the system.

For the second case study we consider sub-cooled jet mixing to control the tank pressure. Once again, an axial liquid jet enters the tank with an average speed of 0.1 cm/s. Here we assume an efficient cryocooler that exists outside of the computational domain can remove enough heat from the liquid so that the incoming jet temperature is maintained at a constant 293 K. In addition to competing with buoyancy-induced flows in the tank, a cold-jet rising into a warmer fluid must also overcome the negative buoyancy of the jet itself before the cooler fluid can reach the interface. Once again, buoyancy effects are reduced in microgravity and the jet's momentum easily carries fluid up towards the interface. A time sequence of temperature and velocity fields is shown in Fig. 7. 90 seconds after activating the jet, the sub-cooled liquid has not yet reached the interface but once cold fluid reaches the interface, the vapor will start condensing and the vapor pressure will drop as indicated in Fig. 10. Once the jet is turned on, the initial sub-cooling is large due to the reduced temperature of the liquid stream. At 90 s, the liquid superheat and sub-cooling are respectively 4.311 K and 14.341 K. As condensation proceeds, and the vapor temperature decreases, the liquid sub-cooling will decrease. After 2 hours of sub-cooled jet mixing, the liquid sub-cooling is now 5.4323 K. As indicated in Figs. 7c and 7d, warm liquid is isolated to regions near the tank wall and at the bottom of the tank away from the ullage. Because these warmer regions of fluid are still being heated from the strip heaters, and the vapor temperature has decreased significantly, the liquid superheat has actually increased during sub-cooled jet mixing. After 2 hours of sub-cooled jet mixing, the liquid superheat is now 8.6849 K. While large superheats increase the likelihood of boiling in the liquid, boiling and its effect on the vapor pressure is currently neglected and will be considered in future papers.

From a power consumption standpoint, it may be inefficient to continuously run a jet mixer. Also, relia-

bility concerns may force the cryogenic community to consider separating the active cooling mechanism from axial jet mixing. So for the next case study, we turn off the jet mixer and use a cold-finger ring submerged in the liquid to provide active cooling. In this case, since the axial jet mixer remains off, any mixing in the liquid is a result of natural convection. A time sequence of the cold-finger cooling case is shown in Fig. 8. 90 seconds after activating the cold finger, cold fluid is localized to the vicinity around the cold-finger ring. Natural convection continues to bring warmer fluid from the side wall up towards the ullage. As time progresses, heat is conducted away from the cold-finger and the region of cold fluid expands. At time = 30 minutes, cooler fluid near the centerline of the tank is shown to be sinking as a result of buoyancy. In addition to the cooler fluid sinking near the cold-finger, the convective flow in the upper half of the tank continues to push fluid down along the centerline. The combined effect, seen at 2 hours in Fig. 8d, is that the cold fluid remains in the bottom half of the tank and never reaches the interface. As such, condensation never begins, and the vapor pressure continues to rise as shown by the vapor pressure history depicted in Fig. 10. Thus, over the 2 hour mixing/cooling period in the ZBOT experiment, cold-finger cooling alone is not an effective means to reduce tank pressure.

To enhance the cooling effect of the cold-finger, for our final case study, we combine cold-finger cooling with axial jet mixing. Once again, no energy is removed between the tank outlet and jet inlet. The axial jet is only used to mix the bulk liquid. The time sequence of temperature and velocity is shown in Fig. 9. After 90 s, the jet has penetrated approximately halfway into the tank, but the coldest fluid in the tank is still localized to regions around the cold-finger ring. As time progresses, heat conducts away from the cold-finger and cooler fluid gets entrained with the incoming liquid stream. Once this cooler fluid reaches the interface the vapor will begin to condense and the vapor pressure will decrease as shown in Fig. 10. It should be noted that the diameter of the cold-finger ring is a very important design parameter. If the diameter of the ring is too small, the jet flow will be blocked from reaching the interface and jet enhancement of cold-finger cooling will be reduced. Similarly, if the diameter of the ring is too large, cold fluid around the cold-finger may not become entrained in the incoming liquid jet and cold-finger cooling with axial jet mixing will not be as effective. Of course, increasing the surface area of the cold finger by adding fins to the ring surface will increase the effectiveness of heat removal, but these finer points of cold-finger design are outside the scope of the ZBOT experiment.

## V. Conclusion

Recent studies suggest that Zero Boil-Off (ZBO) technologies, aimed at controlling the pressure inside cryogenic storage tanks, will play a prominent role in meeting NASA's future exploration goals. Small-scale experiments combined with validated and verified computational models can be used to optimize and then to scale up any future ZBO design. Since shortcomings in previous experiments make validating comprehensive two-phase flow models difficult at best; the Zero Boil-Off Tank (ZBOT) experiment has been proposed to fly aboard the International Space Station. In this paper, a numerical model was developed to examine several test points in the ZBOT test matrix. First an axial liquid jet was used to mix the bulk liquid. Results indicated that after an initial drop in tank pressure, a mixing jet alone is not enough to further reduce tank pressure. Further reductions must be accompanied by removing energy from the system. The introduction of a sub-cooled liquid jet and cold-finger cooling are two strategies under consideration to remove energy from the system and reduce tank pressure. It was shown that over the time scales under consideration, sub-cooled jet mixing is an effective way to control tank pressure but cold-finger cooling is not. To enhance the effect of the cold-finger, an axial mixing jet was introduced into the tank while the cold-finger was active. While pressure reduction was enhanced with the addition of the mixing jet, sub-cooled jet mixing was found to be the most effective strategy under consideration to rapidly reduce tank pressure.

## Acknowledgments

The computational resources provided by the Ohio Supercomputing Center and various post-processing packages provided by the Computational Microgravity Laboratory at the NASA Glenn Research Center are gratefully acknowledged.

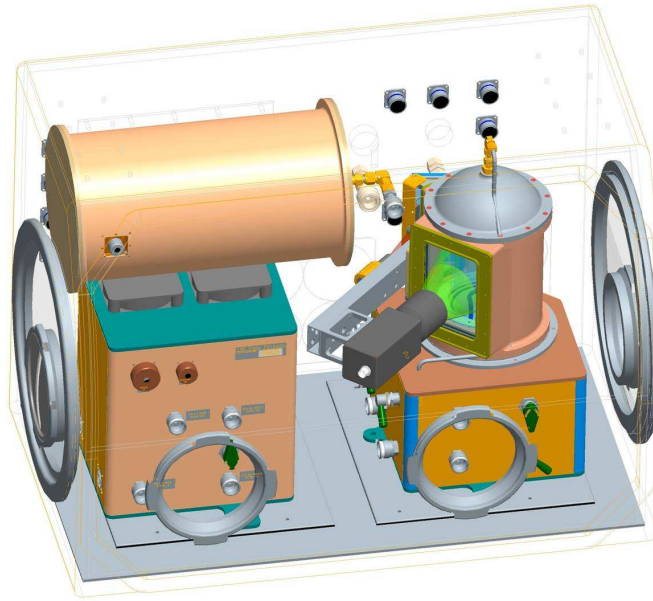
## References

- <sup>1</sup>L. J. Salerno and P. Kittel. Cryogenics and the human exploration of mars. *Cryogenics*, 39:381–388, 1999.
- <sup>2</sup>D. W. Plachta and P. Kittel. An updated zero boil-off cryogenic propellant storage analysis applied to upper stages or depots in an leo environment. AIAA 2002-3589, 2002.
- <sup>3</sup>L. J. Poth and J. R. Van Hook. Control of the thermodynamic state of space-stored cryogenics by jet mixing. *J. Spacecraft and Rockets*, 9(5):332–336, 1972.
- <sup>4</sup>L. J. Hastings, R. H. Flachbart, J. J. Martin, A. Hedayat, M. Fuzah, T. Lak, H. Nguyen, and J. W. Bailey. Spary bar zero-gravity vent system for on orbit liquid hydrogen storage. NASA TM 2003-212926, 2003.
- <sup>5</sup>A. Hedayat, J. W. Bailey, L. J. Hastings, and R. H. Flachbart. Test data analysis of a spray bar zero-gravity liquid hydrogen vent system for upper stages. In *Proceedings of the 2003 Cryogenic Engineering Conference*, 2003.
- <sup>6</sup>D. Plachta. Results of an advanced development zero boil-off cryogenic propellant storage test. AIAA 2004-3837, 2004.
- <sup>7</sup>M. S. Haberbush, R. J. Stochl, and A. J. Culler. Thermally optimized zero boil-off densified cryogen storage system for space. *Cryogenics*, 44:485–491, 2004.
- <sup>8</sup>R. J. Hung and C. C. Lee. Effect of a baffle on slosh waves excited by gravity-gradient acceleration in microgravity. *J. Spacecraft and Rockets*, 31(6):1107–1114, 1994.
- <sup>9</sup>L. D. Peterson, E. F. Crawely, and R. J. Hansman. Non-linear fluid slosh coupled to the dynamics of spacecraft. *AIAA J.*, 27(9):1230–1240, 1989.
- <sup>10</sup>J. C. Aydelott. Axial jet mixing of ethanol in cylindrical containers during weightlessness. NASA TP 1487, 1979.
- <sup>11</sup>J. C. Aydelott. Modelling of space vehicle propellant mixing. NASA TP 2107, 1983.
- <sup>12</sup>S. G. Berenyi, R. C. Nussle, and K. L. Abdalla. An experimental investigation of the effect of gravity on a forced circulation pattern in spherical tanks. NASA TN D-4409, 1968.
- <sup>13</sup>J. C. Aydelott. Effect of gravity on self-pressurization of spherical liquid hydrogen tankage. NASA TN D-4286, 1967.
- <sup>14</sup>M. D. Bentz. Tank pressure control in low gravity by jet mixing. NASA CR 191012, 1993.
- <sup>15</sup>M. M. Hasan, C. S. Lin, R. H. Knoll, and M. D. Bentz. Tank pressure control experiment: Thermal phenomena in microgravity. NASA TP 3564, 1996.
- <sup>16</sup>C. H. Panzarella and M. Kassemi. Analysis of noncondesable gas effects on the evaporative and condensive mass transfer across a liquid vapor interface, *In Preparation*.
- <sup>17</sup>C. H. Panzarella and M. Kassemi. Self-pressurization of large spherical cryogenic tanks in microgravity. *J. Spacecraft and Rockets*, 42:299–308, 2005.
- <sup>18</sup>C. H. Panzarella, D. Plachta, and M. Kassemi. Pressure control of large cryogenic tanks in microgravity. *Cryogenics*, 44:475–488, 2004.
- <sup>19</sup>C. H. Panzarella and M. Kassemi. Comparative analysis of alternative zero boil off pressure control strategies for long duration cryogenic fluid storage in microgravity. *J. Spacecraft and Rockets*, 48:41–68, 2005.
- <sup>20</sup>Y. S. Cha, R. C. Niemann, and J. R. Hull. Thermodynamic analysis of helium boil-off experiments with pressure variations. *Cryogenics*, 33:675–679, 1993.
- <sup>21</sup>C. S. Lin, N. T. VanDresar, and M. M. Hasan. Pressure control analysis of cryogenic storage systems. *J. Propulsion and Power*, 20(3):480–485, 2004.
- <sup>22</sup>C. H. Panzarella and M. Kassemi. On the validity of purely thermodynamic descriptions of two phase cryogenic fluid storage. *J. Fluid Mech.*, 484:41–68, 2003.
- <sup>23</sup>R. W. Arnett and R. O. Voth. A computer program for the calculation of thermal stratification and self-pressurization in a liquid hydrogen tank. NASA CR 2026, 1972.
- <sup>24</sup>S. Gursu, S. A. Sherif, T. N. Veziroglu, and J. W. Sheffield. Analysis and optimization of thermal stratification and self-pressurization effects in liquid hydrogen storage systems - part i: Model development. *J. Energy Resources Tech.*, 115:221–227, 1993.
- <sup>25</sup>S. Gursu, S. A. Sherif, T. N. Veziroglu, and J. W. Sheffield. Analysis and optimization of thermal stratification and self-pressurization effects in liquid hydrogen storage systems - part ii: Model results and conclusions. *J. Energy Resources Tech.*, 115:228–231, 1993.
- <sup>26</sup>S. Venkat and S. A. Sherif. Self-pressurization and thermal stratification in a liquid hydrogen test tank under varying gravity conditions. AIAA 2004-1341, 2004.
- <sup>27</sup>R. J. Hung and K. L. Shyu. Constant reverse thrust activated reorientation of liquid hydrogen with geyser initiation. *J. Spacecraft and Rockets*, 29(2):279–285, 1992.
- <sup>28</sup>G. D. Grayson. Computational design approach to propellant settling. *J. Spacecraft and Rockets*, 40(2):193–200, 2003.

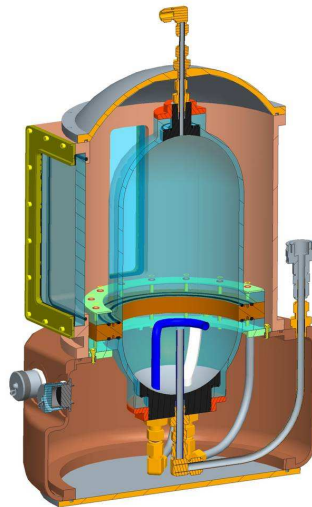
- <sup>29</sup>J. G. Marchetta and J. I. Hochstein. Simulation and prediction of magnetic propellant reorientation in reduced gravity. *J. Propulsion and Power*, 20(5):927–935, 2004.
- <sup>30</sup>A. P. Winter, J. G. Marchetta, and J. I. Hochstein. Simulation and prediction of realistic magnetic positive positioning for space based fluid management systems. AIAA 2004-1151, 2004.
- <sup>31</sup>G. D. Grayson. Coupled thermodynamic-fluid-dynamic solution for a liquid hydrogen tank. *J. Spacecraft and Rockets*, 32(5):918–921, 1995.
- <sup>32</sup>C. S. Lin and M. M. Hasan. Numerical investigation of the thermal stratification in cryogenic tanks subjected to wall heat flux. NASA TM 103194, 1990.
- <sup>33</sup>S. P. Das, S. Chakraborty, and P. Dutta. Studies on thermal stratification phenomenon in lh2 storage vessel. *Heat Transfer Engineering*, 25(4):54–66, 2004.
- <sup>34</sup>A. Sengupta. Comparison of computed to measured liquid hydrogen stratification. In *Proc. of the 2001 ASME Fluids Engineering Division Summer Meeting*, 2001.
- <sup>35</sup>Z. Tanyun, H. Zhongping, and S. Li. *Numerical Simulation of Thermal Stratification in Liquid Hydrogen*, volume 41 of *Advances in Cryogenic Engineering*, pages 155–161. Plenum Press, 1996.
- <sup>36</sup>J. I. Hochstein, H. C. Ji, and J. C. Aydelott. Prediction of self-pressurization rate of cryogenic propellant tankage. *J. Propulsion and Power*, 6(1):11–17, 1990.
- <sup>37</sup>T. J. VanOverbeke. Modeling of pressure reduction due to axial jet mixers in cryogenic tanks. AIAA 2003-998, 2003.
- <sup>38</sup>C.M. Rhie and W.L. Chow. A Numerical Study of the Turbulent Flow Past an Isolated Airfoil with Trailing Edge Separation. *AIAA J.*, 21:1525–1532, 1983.
- <sup>39</sup>S.V. Patankar. *Numerical Heat Transfer and Fluid Flow*. McGraw-Hill, 1980.
- <sup>40</sup>J.H. Ferziger and M. Peric. *Computational Methods for Fluid Dynamics*. Springer, 3rd edition, 2002.
- <sup>41</sup>H.L. Stone. Iterative Solution of Implicit Approximations of Multidimensional Partial Differential Equations. *SIAM J. Numerical Analysis*, 5:530–558, 1968.

**Table 1. Relevant Thermophysical Properties of the System**

Parameter	Value
$\rho_l$	1400 kg/m <sup>3</sup>
$c_l$	1300 J/kg K
$k_l$	0.075 W/m K
$\mu_l$	4.48·10 <sup>-4</sup> kg/m s
$\beta$	0.00219 K <sup>-1</sup>
$M$	0.2 kg/mol
$L$	142000 J/kg
$P_{sat}$ @298K	68900 Pa
$\gamma$	0.0124 N/m
$c_v$	730 J/kg K
$\rho_a$	1190 kg/m <sup>3</sup>
$c_a$	1500 J/kg K
$k_a$	0.2 W/m K
$\rho_{ss}$	7978 kg/m <sup>3</sup>
$c_{ss}$	480 J/kg K
$k_{ss}$	14.2 W/m K
$g$	9.81·10 <sup>-6</sup> m/s <sup>2</sup>



(a)



(b)

**Figure 1. ZBOT experimental configuration: (a) The experimental apparatus inside the Microgravity Science Glovebox. (b) The test cell inside the vacuum jacket.**

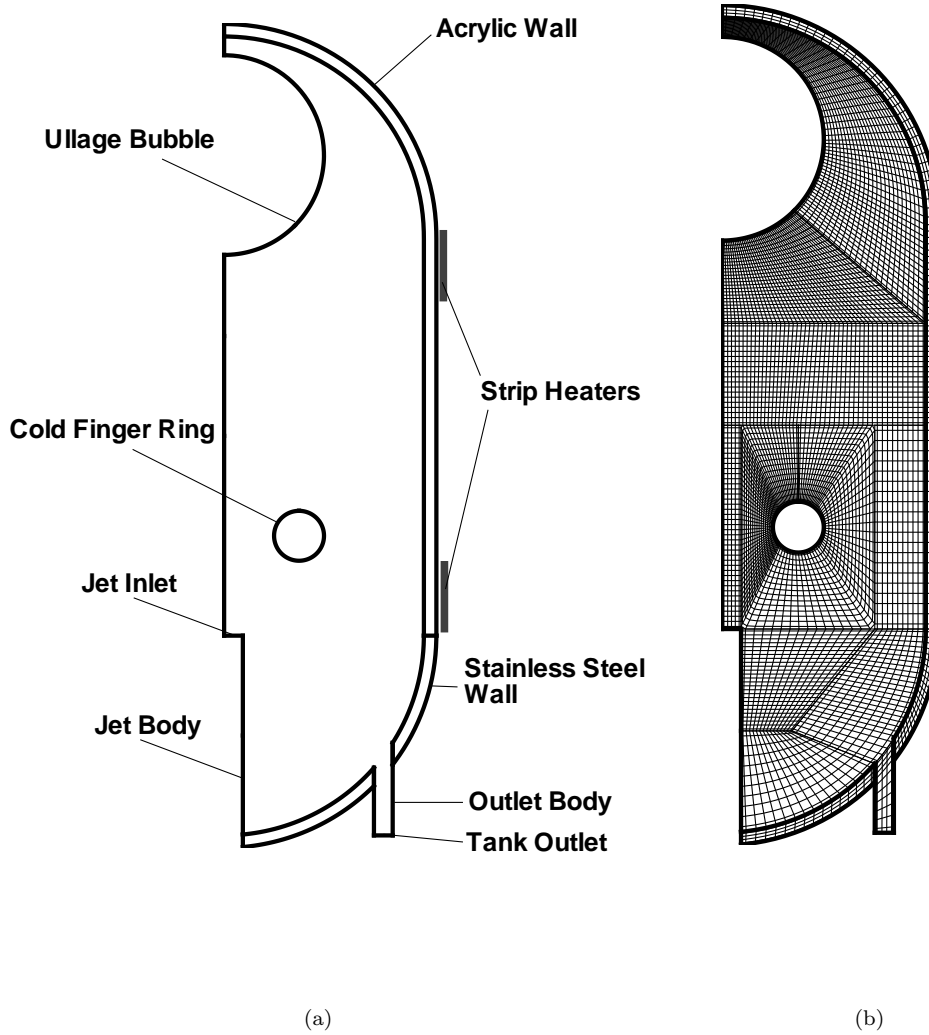
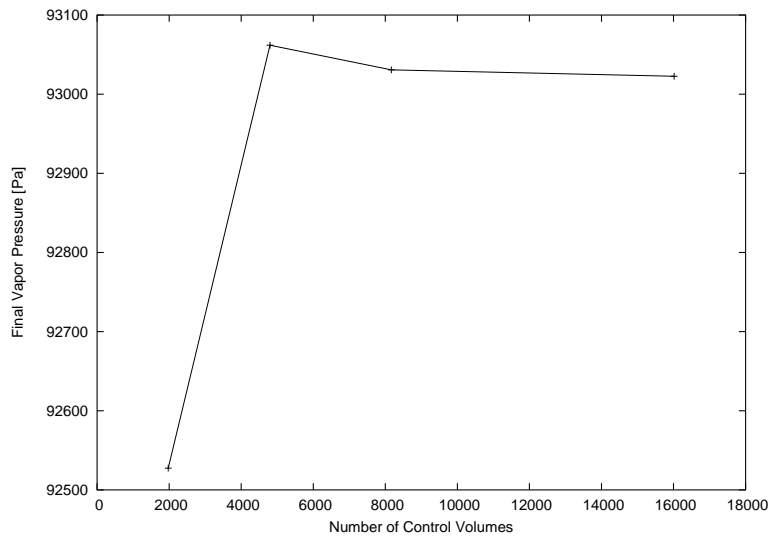
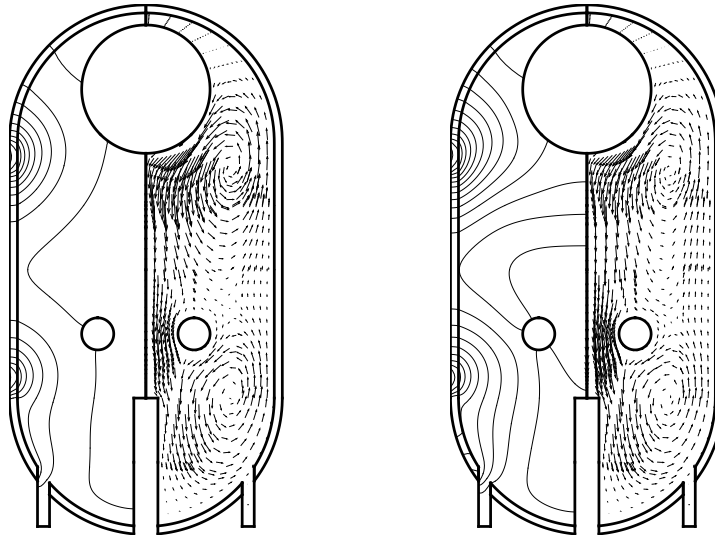


Figure 2. Schematic of the problem geometry (a) and the computational grid (b).

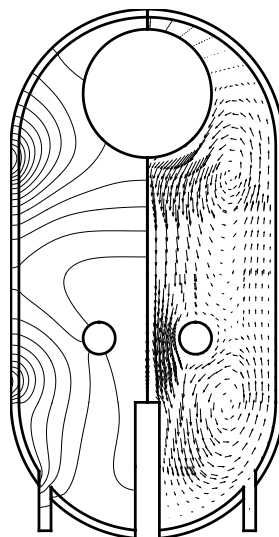


**Figure 3. Grid convergence study.**



(a) 1 hour

(b) 6 hours



(c) 12 hours

**Figure 4. Self-pressurization temperature and velocity histories.**

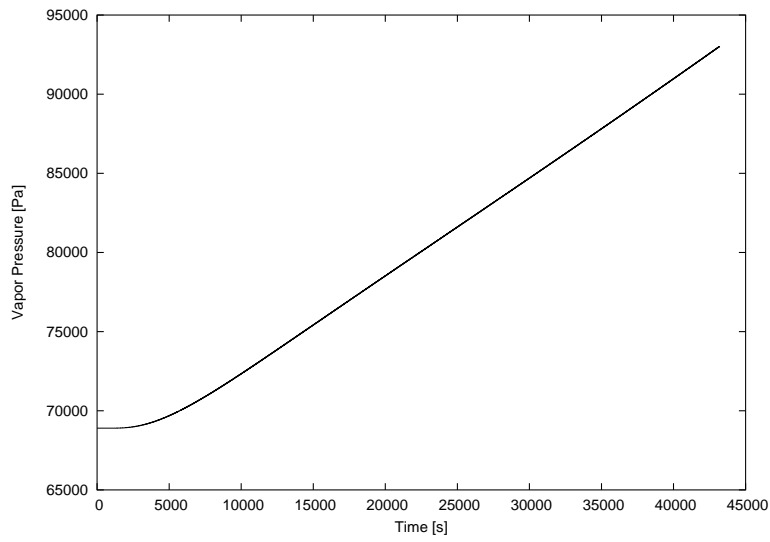
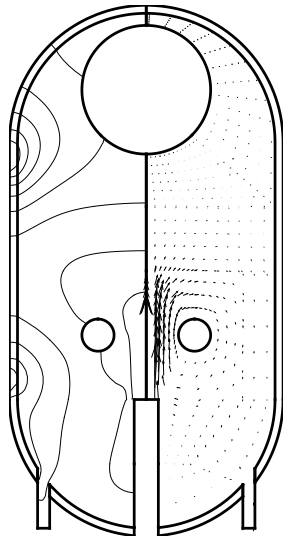
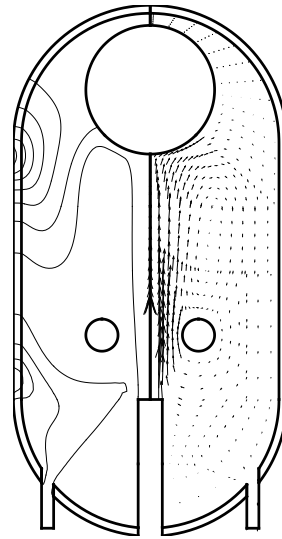


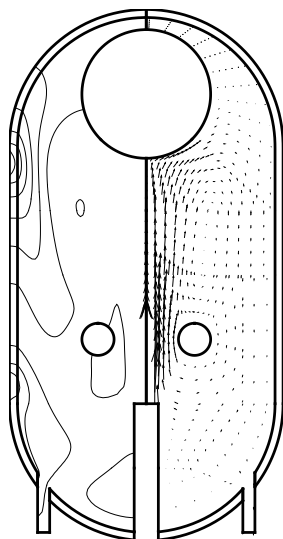
**Figure 5. Vapor pressure history after self-pressurizing for 12 hours.**



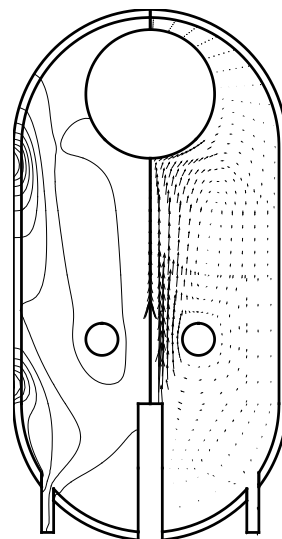
(a) 90 s



(b) 630 s

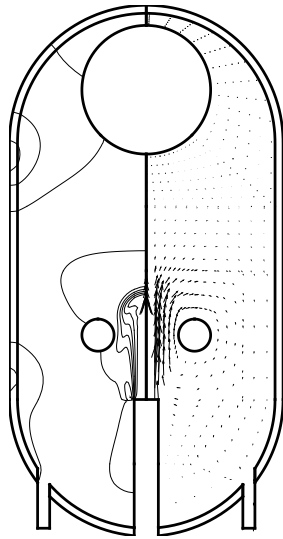


(c) 30 min

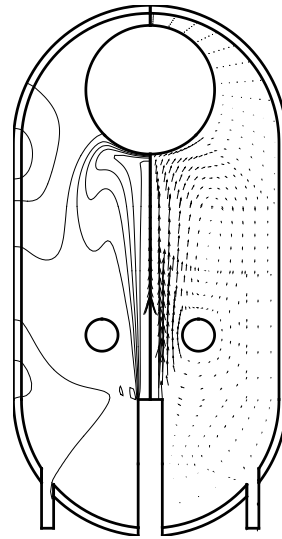


(d) 2 hr

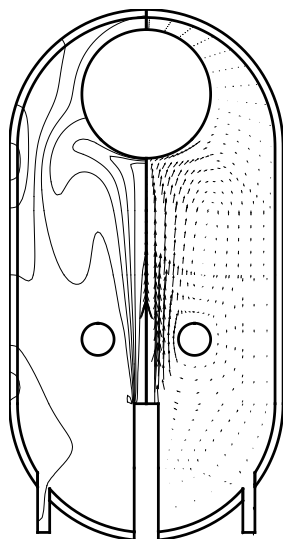
**Figure 6. Sequence of temperature and velocity fields for the axial jet mixing case.**



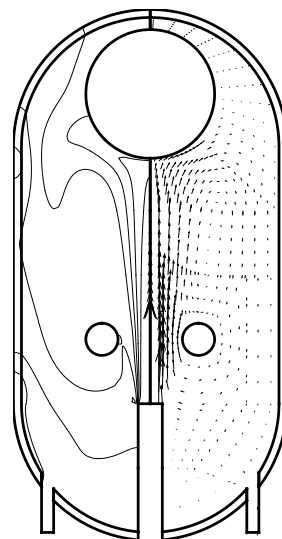
(a) 90 s



(b) 630 s

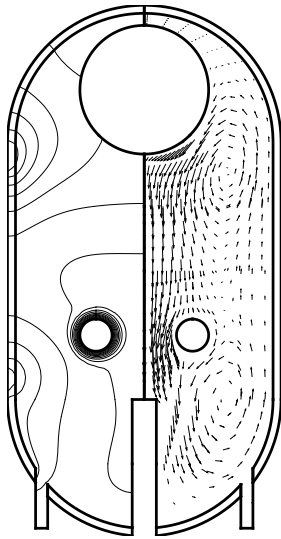


(c) 30 min

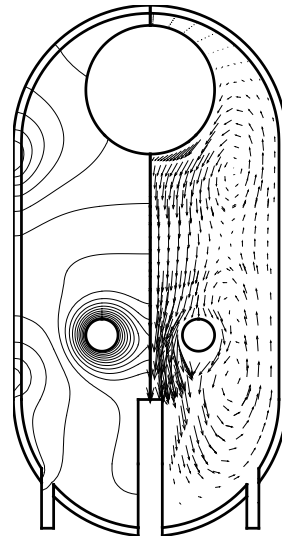


(d) 2 hr

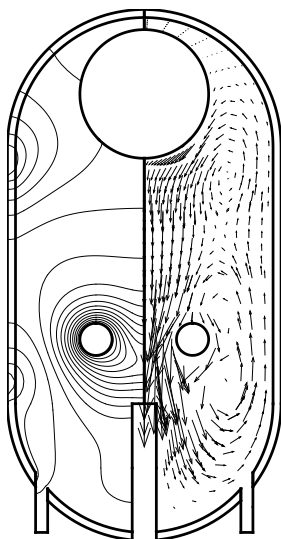
Figure 7. Sequence of temperature and velocity fields for the subcooled jet mixing case.



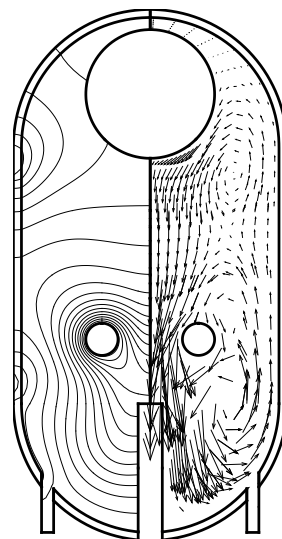
(a) 90 s



(b) 630 s

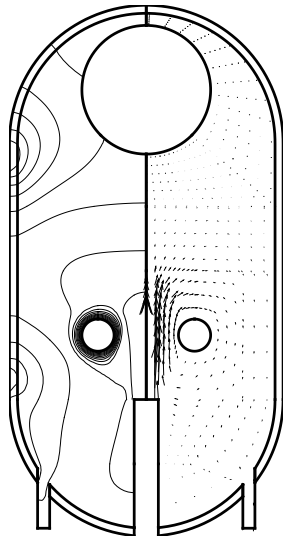


(c) 30 min

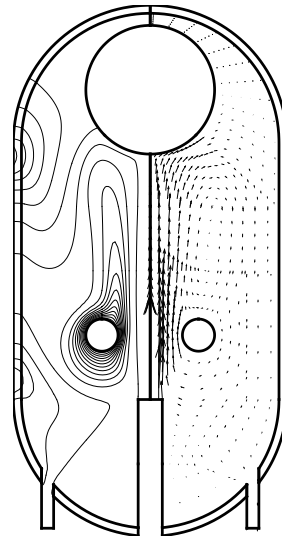


(d) 2 hr

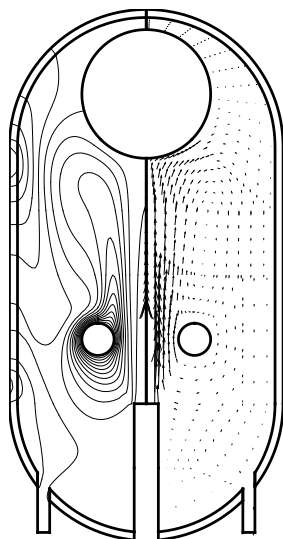
Figure 8. Sequence of temperature and velocity fields for the cold-finger cooling case.



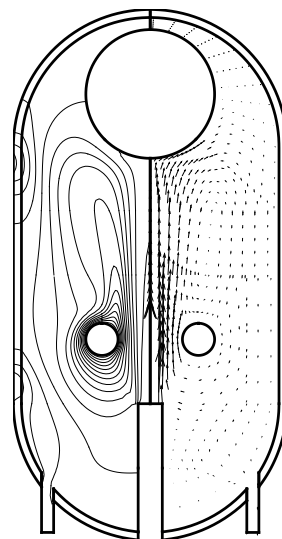
(a) 90 s



(b) 630 s



(c) 30 min



(d) 2 hr

**Figure 9.** Sequence of temperature and velocity fields for the cold-finger cooling + axial jet mixing case.

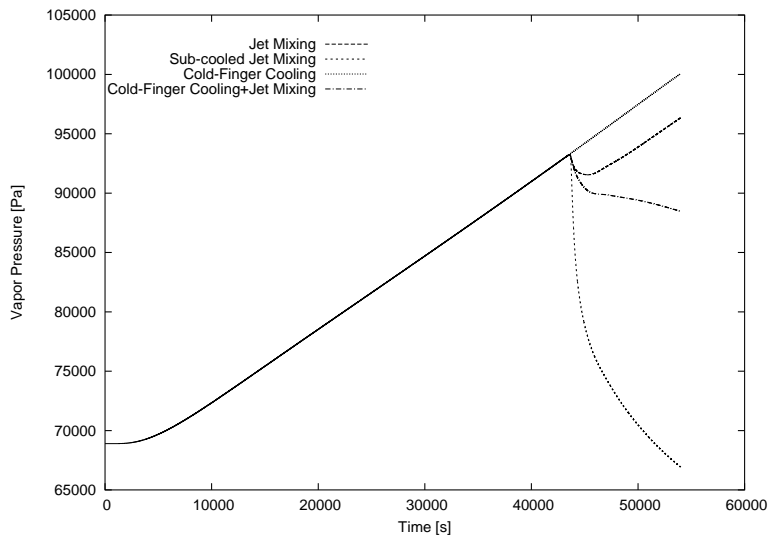


Figure 10. Vapor pressure history.